ADVANCED FUNCTIONAL MATERIALS
www.afm-journal.de

Green Lithography for Delicate Materials

*Artem Grebenko, Anton Bubis, Konstantin Motovilov, Viacheslav Dremov, Evgeny Korostylev, Ivan Kindiak, Fedor S. Fedorov, Sergey Luchkin, Yuliya Zhuikova, Aleksandr Trofimenko, Gleb Filkov, Georgiy Sviridov, Andrey Ivanov, Jordan T. Dull, Rais Mozhchil, Andrey Ionov, Valery Varlamov, Barry P. Rand, Vitaly Podzorov, and Albert G. Nasibulin**

A variety of unconventional materials, including biological nanostructures, organic and hybrid semiconductors, as well as monolayer, and other low-dimensional systems, are actively explored. They are usually incompatible with standard lithographic techniques that use harsh organic solvents and other detrimental processing. Here, a new class of green and gentle lithographic resists, compatible with delicate materials and capable of both top-down and bottom-up fabrication routines is developed. To demonstrate the excellence of this approach, devices with sub-micron features are fabricated on organic semiconductor crystals and individual animal's brain microtubules. Such structures are created for the first time, thanks to the genuinely water-based lithography, which opens an avenue for the thorough research of unconventional delicate materials at the nanoscale.

1. Introduction

Electron beam and deep ultraviolet lithographies (e-beam and DUV, respectively) are among the most reliable micro- and nano-fabrication techniques, delivering device patterning at a high resolution, with a precise match between the design and obtained patterns. However, the conventional implementation of these methods does not permit the fabrication of metal contacts, or any other modification directly on the surface of a wide range of delicate materials. Conjugated organic polymers,[1] small-molecule organic semiconductors (OS),[2] biological materials and nanostructures, such as bacterial[3] and artificial peptide[4] nanowires, hybrid perovskites,[5] metal-organic frameworks (MOFs),[6] organic self-assembled monolayers,[7] and others cannot withstand the chemicals and treatments involved in conventional resist processing protocols. At the same time, existing solvent-less patterning methods, including imprint nanolithography, hard shadow masks, and focused ion beam assisted deposition of metals,[8] impose stringent limitations on resolution, lift-off feasibility and/or require sophisticated fabrication protocols.

There have been several attempts to design e-beam or photoresists based on polyvinyl alcohol[9] and CYTOP, including combinations of the latter with commercial resists,[10,11] which were partially suitable for OS. These techniques, however, require baking of the resist films at 150 °C and additional post-development treatments, such as an oxygen plasma etching, that significantly limit the range of materials compatible with these approaches. Another delicate way was to utilize water-soluble protective layers, such as dextran or polyacrylic acid,

A. Grebenko, A. Bubis, Dr. F. S. Fedorov, Dr. S. Luchkin, Prof. A. G. Nasibulin
Skolkovo Institute of Science and Technology
Nobel str. 3, Moscow 121205, Russia
E-mail: a.nasibulin@skoltech.ru

A. Grebenko, Dr. K. Motovilov, Dr. V. Dremov, E. Korostylev, I. Kindiak, Dr. A. Trofimenko, G. Filkov, G. Sviridov
Moscow Institute of Physics and Technology
Institute Lane 9, Dolgoprudniy, Moscow 141701, Russia

A. Bubis, Dr. R. Mozhchil, Dr. A. Ionov
Institute of Solid State Physics (RAS)
Academician Ossipyan str. 2, Chernogolovka, Moscow 142432, Russia

Dr. Y. Zhuikova, Prof. V. Varlamov
Institute of Bioengineering
Research Center of Biotechnology of the Russian Academy of Sciences
Leninsky Ave.33, bld. 2, Moscow 119071, Russia

The ORCID identification number(s) for the author(s) of this article can be found under https://doi.org/10.1002/adfm.202101533.

DOI: 10.1002/adfm.202101533

Dr. A. Ivanov, R. Mozhchil
National Research Nuclear University MEPhI (Moscow Engineering Physics Institute)
Moscow 115409, Russia

J. T. Dull, Prof. B. P. Rand
Department of Electrical Engineering
Princeton University
Princeton, NJ 08544, USA

Prof. B. P. Rand
Andlinger Center for Energy and the Environment
Princeton University
Princeton, NJ 08544, USA

Prof. V. Podzorov
Department of Physics and Astronomy
Rutgers University
Piscataway, NJ 08854, USA

Prof. A. G. Nasibulin
Aalto University
P.O. Box 16100, Aalto FI-00076, Finland

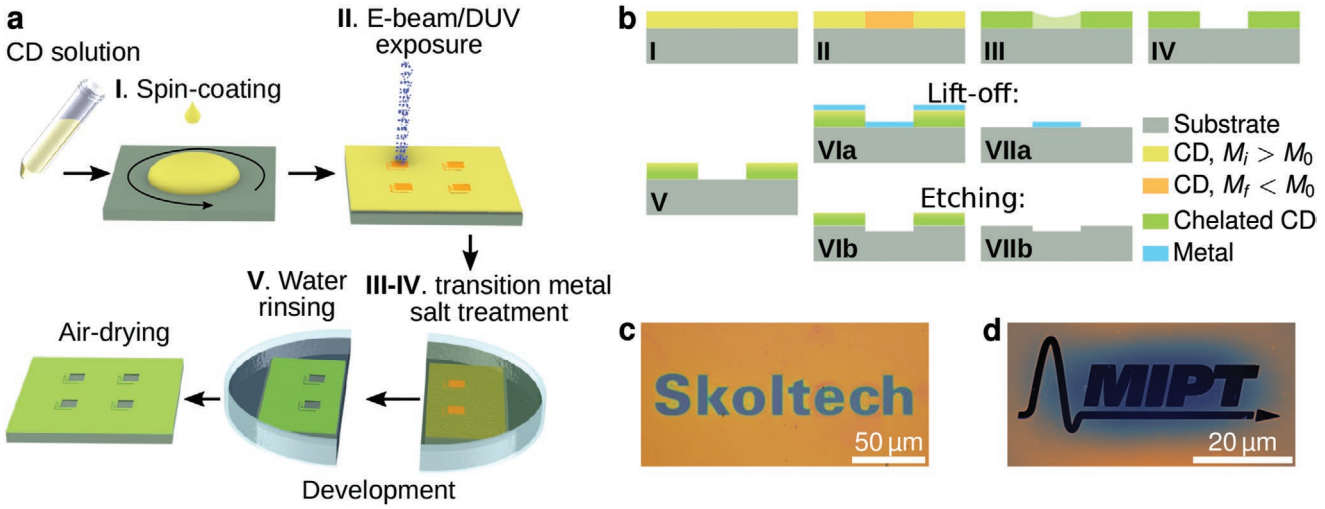

Figure 1. Chitosan based lithography. a,b) A step-by-step procedure for using a CD as a positive-tone resist for lithography. First, an aqueous solution of CD (M_i—initial MW) is spin-coated onto the target substrate/material (I). The film is then exposed to either e-beam or DUV radiation, which results in molecule scissoring and decrease of MW (M_f—final MW) (II). The development process consists of a treatment with an aqueous solution of one or two transition metal salts (developer solutions). Areas of a CD film with MW higher than M_0 (defines boundary for solubility, see Figure 2a) (intact film) is protected from dissolution via chelation reaction, while low MW film ($M < M_0$) (irradiated) starts to dissolve (III). This process ends with completely dissolved CD film in the exposed areas. Non-irradiated areas are chelated throughout the entire film's thickness (IV). Subsequent rinsing in water (V), necessary to wash away by-products, slightly reduces transition element ion content near the surface of the CD film. After the air-drying step, the resist mask is complete. Thus obtained patterned resist film can be utilized in either bottom-up (VIa–VIIa, lift-off application is sketched) or top-down (VIb–VIIb, etching application is sketched) fabrication routines. Film removal is performed in 0.01–0.1% aqueous solution of formic acid (VIIa, VIIb). c) An optical microscope image of a logo patterned in a film of chitosan formate (165 kDa) by an excimer 248 nm laser through an Al mask. d) An atomic-force microscopy image (topography) of a logo patterned in chitosan acetate (65 kDa) film by e-beam.

combined with conventional photo lithographic techniques.[12] Unfortunately, these methods provide poor resolution, and more importantly they are not able to deliver residue-free development, which is the major requirement for further successful processing. In addition, these techniques cannot be extended to e-beam or DUV lithography (because of the detrimental crosslinking of protective layers occurring under exposure), and thus they cannot be used in nanofabrication. One of the first suggested approaches for water-based e-beam and DUV lithographies was to employ a resist made out of fibroin, a protein in a natural silk.[13–15] However, its processing as a resist relies on strong organic solvents and a complex preparation protocol.[16] Further attempts to develop water-based nanolithography used bio-inspired materials, such as a natural linear polysaccharide pullulan (negative tone),[17] chicken egg albumin (both tones),[18] lysozyme mixture with tris(2-carboxyethyl)phosphine (positive tone)[19] and chitosan (positive tone).[20,21] Nevertheless, all of these attempts suffered from a common set of problems: a) the surface of the material of interest within the developed areas of the resist was significantly contaminated with residues and/or b) the intact resist removal was impossible without the use of strong acids, plasma etching, or ionic liquids. Therefore, to the best of our knowledge, there is no genuinely water-based lithography method capable of residue-free development and a bottom-up fabrication (e.g., the lift-off), necessary for working with delicate materials.

The strategy developed in this work is based on chitosan derivatives (CDs), for example, chitosan salts or covalently modified chitosan, serving as the first water soluble, positive-tone resist capable of delivering a reproducible lift-off (bottom-up) and allowing etching (top-down) high-resolution micro- and nano-scale patterns on target substrates. Following the conventional steps of spin-coating and radiation exposure, films of a CD resist are developed in a nearly neutral or moderately acidic aqueous solution of salts of transition metal (d-block) elements (see **Figure 1**). During development, non-irradiated (high molecular weight, MW) areas are protected from dissolution in water by the chelation reaction, while areas exposed to radiation (low MW due to the scissoring) are dissolved and completely removed. A detailed phenomenological model for competing chelation-dissolution development is presented in Experimental Section (see **Figure 2**a). Chelation is a type of bonding between (typically organic) ligands and a metal ion.[22] We emphasize that for the lithographic principle discussed here, it is not really important which particular irradiation source, transition metal salt or CD are used.

2. Resist Development Principle

Onward, we focus on the physical and chemical principles of the e-beam lithography using a chitosan acetate based resist, an aqueous solution of nickel salts used as a model developer and highly diluted formic acid used as a remover (for technical details please refer to Experimental Section). These data can be used by researchers as a starting point for formulating their own custom made developers, resists or removers that would meet the requirements of a particular application of interest. In addition these results can be extended to the use in DUV (Figure 1c) or X-ray lithography. The type of anion (Figure S1, Supporting

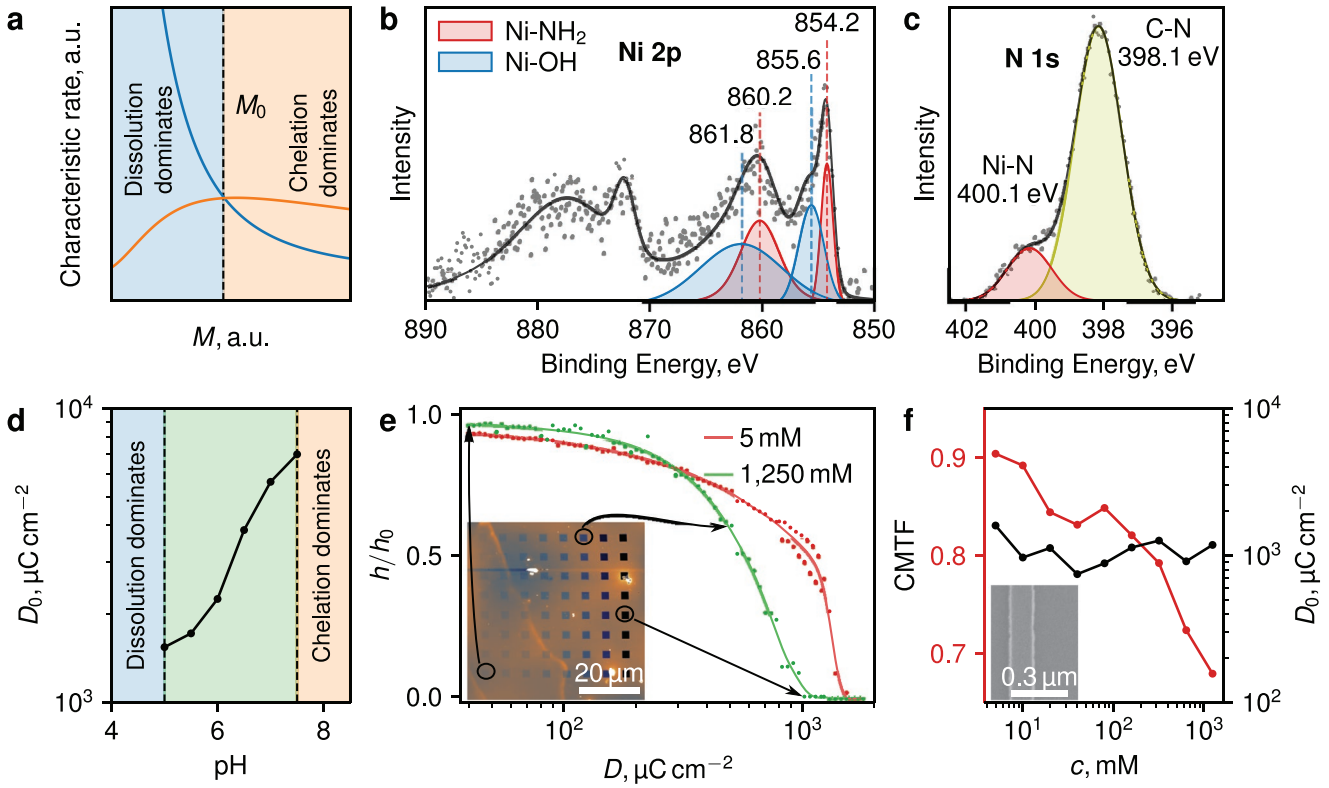

Figure 2. Development of chitosan-based resists. a) Characteristic rates of two competing processes, chelation (orange curve) and dissolution (blue curve) versus molar mass of CD, define the outcome of the development process, where either chelation (faint orange) or dissolution (faint blue) dominates (see Experimental Section for a phenomenological model). b) Ni 2p and c) N 1s core level XPS spectra of unexposed chitosan acetate film processed in $NiCl_2$ solution. d) The dependence of sensitivity (D_0, the minimal radiation dose required for a complete removal of the exposed region) on the pH of developer. e) Height-dose curves obtained by developing with 5 mM (red curve) and 1,250 mM (green curve) $NiCl_2$ solutions. Steepness of these curves is improved with the increase of concentration. Inset: AFM image of the dose-test pixel array sample with exponentially increasing dose of irradiation corresponding to the green curve (particular doses are indicated by arrows). f) CMTF = $(D_{100}-D_0)/(D_{100}+D_0)$, (red line) decreases with increasing concentration, reaching values typical of conventional resists. The sensitivity (black line), on the other hand, is almost independent of concentration. Inset: individual Ti/Pd line obtained via lift-off using high concentration developer.

Information) and the initial MW of chitosan salts (Figure S2, Supporting Information) mostly affect the hydrodynamic properties of the solution and therefore influence spin coating conditions needed to obtain the required thickness, but they do not affect the development process. We have chosen a chitosan acetate with MW = 700 kDa as a representative resist material for electron beam exposure processing. Below we only discuss aqueous solutions of nearly neutral or moderately acidic nickel chloride and sulphate employed as model developers. However, these can be replaced[22] by other transition metal salts (Figure S3, Supporting Information).

The formation of chelate complexes is supported by X-ray photoelectron spectroscopy (XPS) of an unexposed resist film subjected to a 400 mM $NiCl_2$ solution.[23] The Ni 2p (Figure 2b) spectrum is characterized by a spin-orbit doublet (Ni $2p_{3/2}$-$2p_{1/2}$ at 855/872 eV) with satellite structure typical for divalent Ni. A primary Ni $2p_{3/2}$ line at 854.2 eV, followed by a broad satellite peak at 860.2 eV, indicates the formation of Ni—NH_2[24] bonds. Ni—OH bonds are associated with a pronounced shoulder at 855.6 eV and satellite maxima due to multielectron excitation distanced by ≈6.2 eV.[25] Deconvolution of the N 1s spectrum (Figure 2c) reveals two bands with maxima at 398.1 and 400.1 eV, stemming from C—N[26] and Ni—N[24,27] bonds, respectively. The additional nitrogen peak in XPS spectra at ≈400 eV for exposed chitosan was observed after reaction with Ni; it might also be attributed to protonated NH_3^+—Cl^- interaction.[27]

The dissolution of irradiated[28] and non-irradiated[29] chitosan strongly depends on pH of the developer solution, while the chelation rate of Ni[30] is only slightly sensitive to pH. Increasing pH was found to lower the sensitivity D_0, the minimal radiation dose required for a complete removal of the exposed region, as shown in Figure 2d. At a fixed concentration of $NiCl_2$ solution (400 mM) and a set processing time (10 min) chelation reaction dominates for pH > 7.5, preventing the irradiated areas from dissolving for up to the doses of ≈10^5 μC cm^{-2} (which is already sufficient for carbonization of the resist),[31] while at pH < 5.0, the entire film can be completely dissolved at a given concentration due to the boost in the polymer disentanglement process (see Experimental Section and Figure S4, Supporting Information).

Optimization of the transition metal ion concentration in the developer solution improves the overall height-dose curve steepness, which is demonstrated by the difference between 5 (red line) and 1,250 mM (green line) $NiCl_2$ solution used at fixed pH = 5.5 and processing time of 5 min (Figure 2e). The steepness of this curve influences the profile of the developed

structures (the wall angle of the resist), which is of critical importance for the subsequent lift-off of the resist. The general trend for the steepness of the height-dose curve to improve is illustrated in Figure 2f in the form of a critical modulation transfer function (CMTF, red line)[32,33] that depends on the developer concentration, while D_0 is practically insensitive to the Ni ion concentration (Figure 2f, black line). Comparison of the development procedures using CMTF = $(D_{100}-D_0)/(D_{100}+D_0)$, where D_{100} is the maximum dose leading to no changes in the relative height, is more applicable in our case than conventional contrast $\gamma = -d(h/h_0)/d\ln(D)|D = D_0$,[34,35] due to the high nonlinearity of the height-dose curves in a wide range of concentrations (Figure S5, Supporting Information). Such a nonlinearity, that is, the induction effect,[34–36] can be rationalized by the influence of water rinsing stage (see Figure 1b, stage V), during which, a fraction of metal ions escape from the surface, and the near-surface region of the resist partially dissolves, resulting in an inhomogeneous distribution of Ni throughout the film thickness captured by XPS (Figure S6, Supporting Information). In the case of high $NiCl_2$ concentrations, the Ni content in the top layer of the resist is greater, which compensates the loss of Ni ions during rinsing and, respectively, blocks further film dissolution (see Figure S4, Supporting Information).

We found that for a fixed development time of 5 min and pH = 5.5, $NiCl_2$ concentration greater than 1 M, (i.e., CMTF less than 0.7, see Figure 2f) the development yields a reproducible and reliable lift-off with resolution down to 100 nm.

The effect of development salt anion is examined by using a $NiSO_4$-based developer. The solutions containing SO_4^{2-} ions yield a development profile suitable for lift-off at concentrations lower than 200 mM, even though a clean surface in a µm-scale range is harder to optimize for this developer (Figure S7, Supporting Information). The concentration of Ni ions within the thickness of the film is notably greater when compared to the chloride solution, as seen from the XPS measurements (Figure S6, Supporting Information), consistent with an earlier report of the chitosan's sorption capacity.[37] Based on these observations, we formulate one more approach, a two-step development (green line, **Figure 3**a), consisting of consecutive application of $NiCl_2$ and $NiSO_4$ solutions, that is, salts with low and high sorption efficiency. We suggest that the nickel chloride solution impacts mostly the resist residues removal, while high Ni content throughout the resist thickness, ensured through the use of the nickel sulphate, has a major impact on the development profile (see Figure 3) due to decrease of the induction effect (see Figure 3a).

The discussed model solutions reveal that the developer concentration and the type of the anion affect the lift-off process through the improvement of the developed resist wall angle, while the pH of the solution determines the sensitivity. The detailed specific recipes are given in Experimental Section, and their performance is shown in Figure S8, Supporting Information.

3. Patterning of Delicate Materials

To show the extended applicability of the proposed technology, we have employed an e-beam lithographic patterning on the

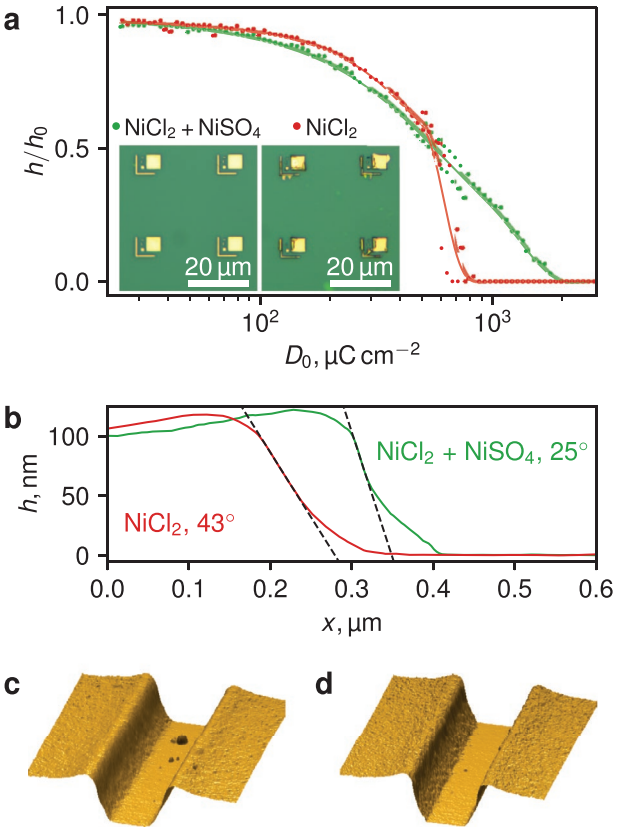

Figure 3. The effect of developer anion. a) The height-dose curves for one-step (red symbols) and two-step (green symbols) development procedures. The inset shows optical microscope images illustrating the difference in the lift-off of the patterned structures. b) Representative AFM profiles of developed lines. The two-step development process results in a smaller angle of developed resist walls. c,d) A 3D rendering of AFM topography of the lines developed via one-step and two-step development processes, respectively. For all presented structures, resist thickness was ≈100 nm.

surface of several prototype OS. These materials, typically van der Waals molecular crystals, are characterized by delicate surfaces prone to thermal or chemical degradation via formation of defects either due to sublimation of surface molecules, their fast dissolution in organic solvents or as a result of their interaction with the ambient environment. Such sensitivity makes many OS largely incompatible with conventional lithographic processing. For this reason, contact structures are usually first prepared on Si/SiO_2 wafers or other substrates, followed by deposition of OS films. This approach, however, has a number of limitations, and direct deposition of high-resolution (lithographically defined) contacts on the surface of OS is highly desirable. We have successfully carried out development and lift-off directly on the surface of single-crystalline OS tetracyanoquinodimethane (TCNQ)[38] using chitosan based resists (**Figure 4**a,b). Well-defined molecular steps, characteristic of organic single-crystal surfaces, can be observed in the developed regions of the resist and under the subsequently evaporated palladium (Pd, see Figure S9, Supporting Information) layer. Exposure of a bare surface of TCNQ crystals to e-beam at the same dose and the subsequent processing in $NiCl_2$ aqueous solution does not

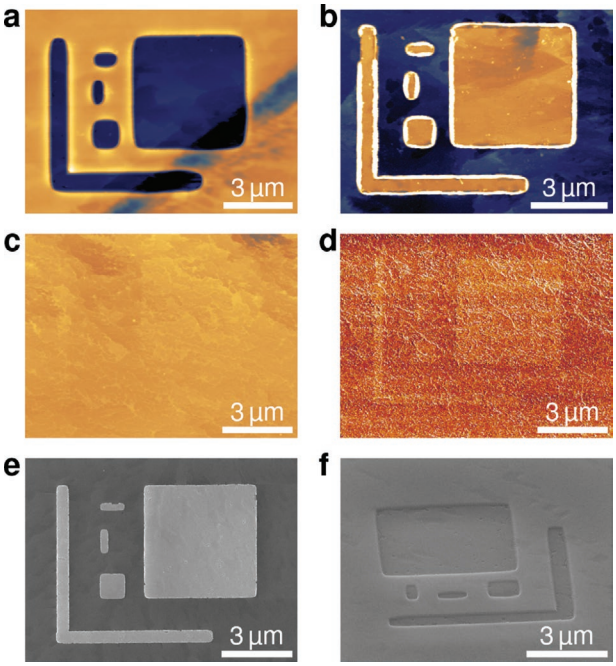

Figure 4. Lithographic patterning directly on the surface of OS. a) An AFM image of the developed area in the resist on the surface of a TCNQ crystal. b) An AFM image of a similarly processed region of TCNQ crystal after the deposition and lift-off of a Pd film. c,d) AFM topography and phase images of the surface of TCNQ single crystals exposed to the same doses as in (a) and (b) and processed by developer solution. SEM images of e) lifted-off Pd structures and f) oxygen plasma etched pattern fabricated on the surface of a rubrene thin film. For all presented patterns, ≈100 nm resist film and irradiation dose of ≈2000 μC cm^{-2} were used.

lead to any significant degradation of morphology (Figure 4c), with only a slight modification of the exposed regions visible in atomic force microscope (AFM) phase scans (Figure 4d). We have also performed a successful lift-off patterning of metallic contacts and oxygen plasma etching on the surface of highly crystalline and compact ultra-thin (≈20 nm) rubrene films that have macroscopic grain size of up to ≈0.5 mm grown on polyimide substrates[39,40] (Figure 4e,f). Both OS used in this study, as well as many others, are stable[41,42] under the processing conditions during the treatment by the developer and remover solutions (see Experimental Section).

4. Electrical Devices

In order to demonstrate lithographic contact fabrication directly on the surface of delicate materials, we used our water-based lithographic technique and fabricated top-contact field effect transistors (FETs) on very delicate materials (see Figure S10, Supporting Information, for devices schemes): individual single-wall carbon nanotubes and rubrene thin films. In the case of SWCNTs,[43] their small diameter makes this system highly sensitive to resist residue, which makes the lithography process challenging[44] in terms of the cleanliness of the developed areas. On the other hand, OS are very sensitive to solvents used in standard semiconductor processing.

For the FET fabrication, we have synthesized SWCNTs by an aerosol (floating catalyst) CVD method[45] and deposited them onto thermally oxidized (300 nm-thick SiO_2) Si wafers (**Figure 5**a,b). By performing chitosan-based e-beam lithography, we have obtained 24 individual SWCNT FETs exhibiting as-fabricated transconductance characteristics similar to those reported previously[46] (Figure 5a,b). More than 60% of the fabricated devices exhibited the ON-state source-drain resistance in the range 10–100 kΩ, which is comparable to the ON resistance of devices fabricated with the standard lithographic approaches[47] but has never been reported for a water-based lithography.

Next, we have successfully fabricated several top-contact/bottom-gate organic FETs (OFETs) using crystalline rubrene thin films grown on polyimide substrates.[39] We have intentionally chosen very small channel lengths in the range $L = 0.6–2.2$, μm, and very narrow metallic electrodes with the width of 0.2 μm in order to demonstrate the potential of this chitosan-based lithography in nano- and microstructure fabrication (inset in Figure 5c). The resultant devices with Pd source and drain contacts show typical diode-like $I–V$ characteristics at zero gate bias (Figure 5c) and exhibit FET characteristics with linear and saturation carrier mobilities[48] in the range of $\mu = (2–3) \times 10^{-3}$ cm^2 V^{-1} s^{-1} (Figure 5d). These mobilities are comparable to the case of staggered geometry (see Figure S10, Supporting Information) FETs on thin-film rubrene.[39,40] Such top-contact/bottom-gate (staggered) geometry leads to the accumulation channel formed at the bottom of the rubrene film, right at the interface with a 5 nm-thick amorphous tris[4-(5-phenylthiophen-2-yl)-phenyl]amine (TPTPA) underlayer used in these devices for better morphology of polycrystalline rubrene films.[39] Additionally, the staggered geometry and Schottky barriers at the Pd/rubrene interface likely lead to a high contact resistance resulting in contact-dominated devices,— a problem that is especially severe in the short-channel FETs fabricated here. Nevertheless, we have achieved our current goal of successfully demonstrating a lithographic fabrication of submicron size channels directly on the surface of OS utilizing our novel chitosan-based lithographic approach.

Finally, we have lithographically defined four-probe contact structures directly on porcine brain microtubules (see **Figure 6**a and Figure S10, Supporting Information). These contacts are made of chromium (1 nm) and palladium (24 nm) and are separated by 50–100 nm-wide gaps. Thanks to the delicate nature of our genuinely water-based lithographic approach, there is no damage of the microtubules discernible in AFM imaging, and the devices remain reproducibly electrically active. We have performed electrical measurements of these brain microtubules in the frequency range 0–8.5 GHz by using an impedance and vector network analyzers (VNA). Figure 6b shows the electric-field transmission spectra region of 7–8.5 GHz, where the microtubule shows one of its characteristic resonances,[49] and the signal can be confidently distinguished from the substrate (see Figure 6 and Figure S11, Supporting Information). We have observed a narrow (≈0.1 GHz) Lorentzian-like electric field absorbance line at 7.2–7.8 GHz in three different samples (see Figure S11, Supporting Information) that appeared to be sensitive to the external conditions, such as the relative humidity varied between 22 and 95% and temperature varied between 22 and ≈38 °C. The observed narrow absorption line[49] can be

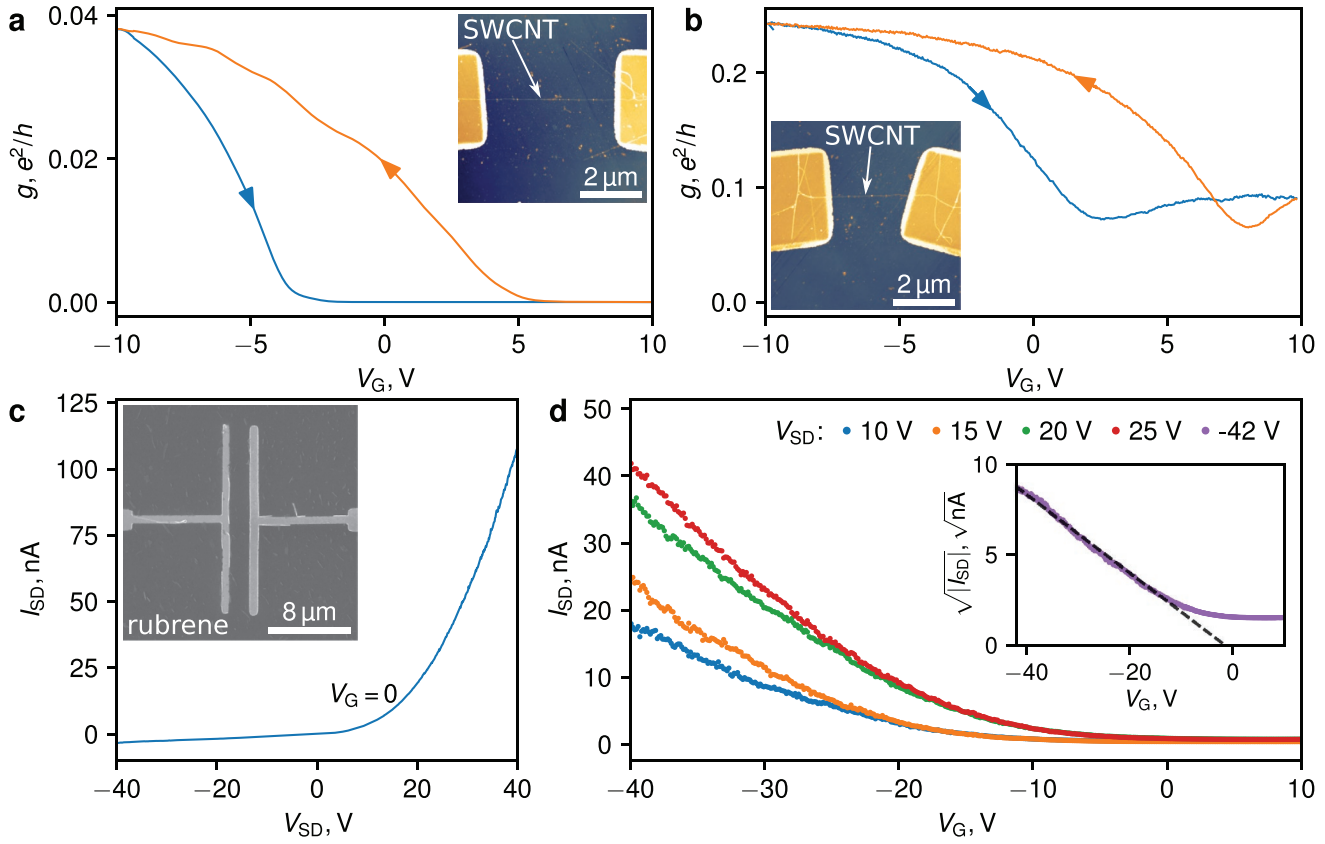

Figure 5. FET devices fabricated directly on delicate materials by means of water-based chitosan lithography. Transconductance characteristics of individual SWCNT FETs demonstrating a) semiconducting and b) metallic/semi-metallic behavior. The insets are AFM images of the corresponding structures with SWCNTs indicated by arrows. c) I_{SD} (V_{SD}) at $V_G = 0$ of a polycrystalline rubrene OFET with a 2 μm-long channel, exhibiting a diode-like behavior. Inset: SEM image of the source-drain contact structure. d) The transfer I_{SD} (V_G) characteristics of the same OFET in the linear regime. The inset shows a transfer characteristic of the device in the saturation regime. All devices were fabricated using 100 nm chitosan acetate film and ≈2000 μC cm^{-2} dose.

attributed to the propagation of a kink soliton wave of dipole polarization travelling along the microtubule,[50,51] as theoretically predicted earlier by Hameroff and Penrose.[52] The role of the microscopic surrounding of the microtubule, including water at its surface, as well as the effect of temperature, can be described by various models of propagation of such waves.[50] Broadband dielectric response (including GHz range) of biological macromolecules is generally highly sensitive to the level of hydration and temperature. Usually, increasing temperature and elevated level of hydration both lead to a blue-shift in the observed relaxations.[53,54] In many protein systems, high-temperature charge dynamics is governed by the fundamental frequency–temperature superposition principle clearly demonstrated by corresponding scaling curves.[55] Here, thanks to the proposed lithographic approach, we demonstrate the possibility of fabrication of damage-free, electrically active devices, which opens the pathways for further detailed investigation of such biological micro- and nano-objects.

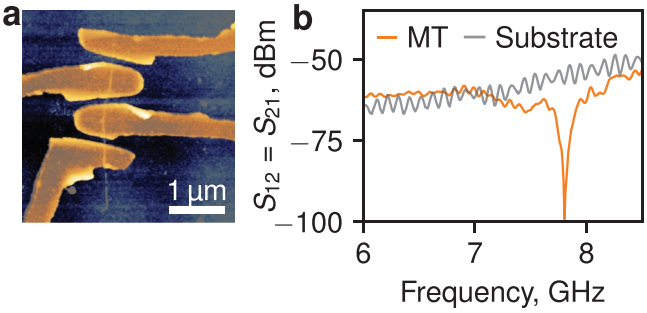

Figure 6. The electric field transmission through an individual porcine brain microtubule. a) A false-color AFM image showing a four-probe structure lithographically patterned directly (through 100 nm chitosan acetate film) on top of the microtubule. b) The parameters S_{12} and S_{21} of the scattering matrix defining the transmission of electric field through the microtubule. Measurements were carried out at 38 °C. Only the high-frequency range, containing one of the resonances relevant to the microtubule, is shown for simplicity. The sample with the microtubule (the orange line) is compared to the signal of its substrate (the grey line).

5. Conclusion

To conclude, we have developed here a genuinely water-based positive-tone e-beam and DUV lithographic technique capable of bottom-up (lift-off) approach, where the resist is made out of CD. The proposed technology employs specific chelation chemistry of chitosan and yields a competitive quality of resist development, both in terms of the negligible surface contamination

and the developed resist wall's angle. This fact is most clearly confirmed by the competitive quality of the obtained SWCNT-based devices. Furthermore, this method is shown to be compatible with the surface of delicate materials, where it results in reliable fabrication of nano- and micro-scale contacts to OS, such as rubrene and TCNQ, as well as small biological objects—brain microtubules all of which are completely incompatible with the conventional lithography techniques. The demonstrated water-based lithography opens further opportunities in research, development, and applications of micro- and nanostructures based on delicate OS, monolayer materials, MOFs, biological objects (proteins, DNA, etc.), as well as conjugated polymers. It is a major leap forward in the evolution of water-based lithography techniques due to the high quality development, the possibility of both the bottom-up (lift-off) and the top-down (etching) fabrication at 100 nm resolution, and compatibility with a wide range of emergent materials, all demonstrated here for the first time. The employed resist materials and processes are extremely cheap, free from any harsh or toxic chemicals, severe temperature treatments or other aggressive conditions, which makes this technology applicable to a much wider range of materials compared to the modern commercial resists.

6. Experimental Section

CD: Chitosan Salts of Organic Acids: The performance of various salts of chitosan were analyzed, including chitosan acetate, formate, lactate, glycolate, and succinate. The best lift-off performance was observed with chitosan acetate, formate, and glycolate. Carboxymethyl chitosan[56] and chitosan phthaloyl[57] were also tested (not shown), which provided a lift-off capable patterning as well as salts following the same development protocol. All of them exhibited merely similar behavior; the best results are presented in Figure S1, Supporting Information.

The method of the derivative synthesis did not affect the final result. The tested methods could be classified into two main groups depending on the need in the amount of the final product:

- Industrially feasible method: In a round bottom glass flask the solution consisting of 29 mL of H_2O and 480 mL of ethanol was prepared. Afterward the subsequent 75 mL of organic acid in the concentration of roughly 60% was added. The mixture was stirred for 1 min. Then 100 g of pure chitosan was added and heated to 50 °C. The obtained blend was stirred for 3 h and cooled down to room temperature. The sediment was filtered and transferred back to the flask with 400 mL of ethanol. Then the mixture was stirred at room temperature for 10 min. The sediment was again filtered and washed two times on the filter by using 40 mL of ethanol followed by drying for 12 h at ambient conditions. Then the sediment was transferred to a round bottom flask and dried on a rotary evaporator for 6 h at the residual pressure of 15 mbar and the heating temperature of 50 °C. By this method, chitosan acetate, formate, glycolate, succinate, lactate, chloride, and citrate were obtained with a MW of ≈165 kDa.
- Lab scale method: Chitosan acetate of 20 and 65 kDa samples were obtained by chemical hydrolysis in a nitric acid.[58] To get the samples with the weight of 80 kDa, a fermentative hydrolysis[59] was applied and for the samples with MW of 200 and 700 kDa precipitation purification was performed. For this, 1% solution of chitosan in 1% acetic acid was prepared, and then this solution was centrifuged at 5,000 rpm for 10 min to separate undissolved precipitate followed by adding of 12% solution of NH_4OH to tune the pH value to 8.5. The solution was centrifuged at 6,000 rpm for 15 min. The precipitate was washed twice with distilled water, dialyzed for 3 days and freeze-dried. Each sample (100 mg) was suspended in 25 mL of distilled water and transferred to acetate form by titration in 1% acetic acid under rigorous stirring until pH reached 4.0 and complete dissolution of the sample (complete protonation of chitosan amino-groups). The solution was dialyzed for 3 days and freeze-dried.

Radiation Exposure: For DUV experiments, CL7100 (Optosystems Ltd.) KrF excimer laser was used with 248 nm wavelength and the laser pulse duration of 20 ns. The energy of the pulse was controlled using LabMax-TOP Laser Power/Energy meter with energy sensor J-50MUV-248. The irradiation was performed at a fluence of 20 mJ cm^{-2} per pulse at a repetition rate of 11 Hz for a fixed number of pulses. To form a pattern Al mask on UV-transparent fused quartz was fabricated by the means of e-beam lithography and ICP chlorine etching. Mask was fixed on top of the substrate by a 3D micro-mechanical manipulator for exposure. The approximate dose required for complete development of the exposed region was 1000 pulses. E-beam lithography was done on Crestec CABL 9000C lithography system. The accelerating voltage was kept constant at 50 kV value. Probe currents varied in range from 50 pA to 10 nA, which led to covered dose range from 25 to 150 000 μC cm^{-2}.

Microscopy: Leica DM4500 P LED optical microscope combined with a digital camera was used to analyze the results of the development or lift-off. For more detailed studies of chitosan films morphology, thickness, exposed areas shape, residues quantity, mechanical film properties after various treatments, Bruker Multimode V8 Atomic Force Microscope in ScanAsyst-Air, PeakForce-HR, and Quantitative NanoMechanical mapping modes were used. Cypher ES microscope (Asylum Research, CA) was also used in tapping mode. Usually soft tips with a spring constant of 0.4 N m^{-1} were used. SEM images were obtained at Jeol JSM-7001F at acceleration voltages from 10 to 30 kV.

X-Ray Photoelectron Spectroscopy: XPS spectra were collected by XPS spectrometer Kratos Axis Ultra DLD with spherical sector analyzer, ion gun, UV, and X-ray sources. Experiments were conducted under ultra-high vacuum $5{\cdot}10^{-10}$–$3{\cdot}10^{-9}$ Torr utilizing the irradiation of AlKα(mono) 1486.69 eV (energy resolution 0.48 eV, binding energy calibration on Ag $3d_{5/2}$ line and C 1s).

Chelation-Dissolution Development Concept: For the classical resist development[36] dissolution rates of the irradiated and pristine resist R_f and R_f are governed by $R_f/R_i = (M_i/M_f)^{\beta}$, where β is the solubility factor and M_f and M_i are the MW of the irradiated and pristine sample, respectively. The solvent, used as a developer, is chosen to increase the solubility factor β, but, at the same time, it is chosen as a weak solvent of a corresponding intact polymer. In order to obtain residue free development, strong solvent was proposed for the CD considered in this work—water. This requires an unconventional positive developer that would inhibit dissolution of the unexposed parts of the film in an aqueous developer solution, and to do so, a reaction of chelation of the CD with transition metal ions was employed.[22,60] The resulting CD chelate complexes were much less soluble in water compared to its pristine form. Irradiation of chitosan and its derivatives with either UV light, X-ray, or electron beam leads to a decrease in MW that depends on the irradiation dose,[61–64] D: $1/M_f$–$1/M_i \propto D$. This process was accompanied by a local heating and liberation of gaseous H_2 and NH_3[64] that resulted in a noticeable thinning of the resist film (Figure S12, Supporting Information). The rate of both processes, the dissolution in water and chelation with transition metal ions, depends on the CD molecular weight. The diffusion lag time[65] τ, of these two reactions could be used to qualitatively distinguish the characteristic time scale of disentanglement responsible for dissolution, τ_{dis}, and the time scale of chelation, τ_{chel}. The processes was considered occurring at the length scale of the polymer's gyration radius, $r_g \propto M^{1/2}$, and thus $\tau \propto r_g^2/D_{diff}$, where D_{diff} is a diffusion coefficient for the particular process. For dissolution, according to the scaling model of polymer disentanglement,[66] the coefficient of self-diffusion of a polymer with molecular weight M is $D_{self} \propto 1\ M^{-2}$, which gives $\tau_{dis} \propto M^3$. In the case of chelation, the model of membrane ion mobility[67] predicted the diffusion

coefficient to be $D_{chel} \propto \exp(-1\ M^{-2})$ and therefore $\tau_{chel} \propto M \exp(1\ M^{-2})$. Both of these time constants, τ_{dis} and τ_{chel}, and therefore the respective diffusion rates, $R \propto 1/\tau$, depend on the characteristics of the developer solution that can be tuned to reach the situation depicted in Figure 2a. Two *M*-dependent characteristic process rates cross at a value M_0, corresponding to the MW below which the dissolution process is faster than the formation of the chelate complex, while for heavier molecules chelation dominates, preserving the high-*M* regions of the resist. For a particular transition metal salt developer solution the sharpness of the rate dependencies on *M*, and the position of M_0 can be varied by the solution pH, concentration of the transition metal ion or the type of anion.

Developer and Remover Constituents: $NiCl_2$ (99.9%) and $NiSO_4$ (99.9%) were purchased from RusHim company (Moscow, Russia) and used without any additional purification. Fresh developer solution was prepared before each experiment. $NiCl_2$ and $NiSO_4$ salts were dissolved in MQ water at a concentration of 5–5000 mM and their pH was adjusted by HCl and H_2SO_4 to reach the desired value. All developments were carried out in dishes/six-well plates fixed on the orbital shaker working at 200 rpm under 22 °C and RH from 25 to 45%. For one-step development, the sample was first transferred into nickel chloride solution for 5–10 min, afterward moved to the MQ water on the same orbital shaker for 30 s and finally air dried. For two-step development the first step is 5 min treatment in 200–400 mM $NiCl_2$ water solution with pH = 5.5. Then the chip is transferred into 200–400 mM $NiSO_4$ water solution with pH = 5.5 for additional 5 min. Finally, the chip is rinsed in MQ water for 30 s. As a remover highly diluted (0.01–0.1% vol.) formic acid, an eco-friendly food additive was mainly used, which resulted in fast (≈1 min) lift-off and low residues on substrate surface. The $NiCl_2$ solution used in the presented research is a Ni^{2+} salt formed by interaction of the weak base $Ni(OH)_2$ (solubility constant of 6×10^{-18} in water) with a strong acid HCl. Until reaching high concentration values of an order of several M, the resulting solution has a slightly acidic pH, close to neutral in the range 5–7. For the case of highly concentrated solutions this value can be as low as 4. In general, it is also valid for the case of other transition element ions presented in this study. Co and Ag also produce merely neutral solutions. In any way the solution's pH can and should be tuned by addition of the corresponding base or acid in order to facilitate the sweet-point of the two competing reactions: dissolution and chelation. Ni^{2+} cation is neither a strong oxidizing nor a strong reducing agent with the standard potential of $E_0 = -0.25$ V for the half-reaction $Ni^{2+} + 2e = Ni^0$. Several metals were tested in terms of compatibility with the suggested protocol, including reactive Al and rather unstable Ti, which were not affected by our lift-off protocol in 0.1% formic acid. Most widely used substrates (like Si, SiO_2, Si_3N_4, GaAs, etc.) as well as typical metals (like Ti, Al, Au, Cr, etc.) were not damaged following our protocol.

Optimized Lift-Off Lithography and its Performance: To study the development process, a chitosan acetate solution was spin-coated onto commercially available Si wafers with a 300 nm-thick thermal SiO_2. The films were then exposed to a matrix of rectangular test structures (inset in Figure 2e) with gradually increasing radiation dose (denoted throughout the text as dose-test pixels). The developed dose-test pixels were studied by AFM, and the height-dose curves were obtained after the processing. The dependence of sensitivity was investigated, D_0, as well as the shape of the height-dose curves on the pH, the concentration, and anion type of the transition metal salt developer solution (see Figure 2 and Figure S5, Supporting Information).

Two major approaches could be formulated that could deliver a lift-off capable development (Table S1, Supporting Information). The first approach was to utilize a high-concentration developer based on $NiCl_2$ (1–5 M solution, at pH 3–5, and processing time from 5 to 10 min, followed by 30 s water rinsing), which provided a clean development of the exposed regions (Figures S8a and S7, Supporting Information), a reproducible lift-off (Figure S8b, Supporting Information), an outstanding 100 nm resolution (Figure S8c,d, Supporting Information), and high sensitivity of ≈130 μC cm^{-2}. The second recipe targeted to lower the chemical reactivity of the developer solution by combining two nickel salts. This approach enabled lowering of the developer concentration down to hundreds of mM at pH 5.5 (the same processing and rinsing time), while keeping the sensitivity at the order of 2000 μC cm^{-2}. Developed and lifted-off structures obtained by the two-step approach are shown in Figure S8e,f, Supporting Information. However, the narrowest metal line obtained by two-step development and lift-off is limited to 250 nm (an array of such lines with a 1 μm period is shown in Figure S8g,h, Supporting Information).

Successful realization of the lift-off process also required a proper solvent to remove the non-exposed film after the deposition of desired material (for instance, metal for contacts). The water itself could be used as a remover, but it might take up to several days to complete the process after chelation. It was found that aqueous solutions of weak organic acids, specifically a 0.01–0.1% formic acid solution, is an effective remover, because it provided a rapid film dissolution, clean substrate in the regions previously covered by unexposed film, and it was compatible with a wide range of materials including organic and biological substances, carbon-based nanomaterials and metals.

Deposition and Etching: For deposition of metal films, two evaporation systems were utilized: thermal evaporator Tecuum AG with a base pressure of $1–5\cdot10^{-6}$ Torr and electron beam evaporator Angstrom with base pressure of $1–5\cdot10^{-7}$ Torr. Plasma etching of OS was performed in Diener Nano plasma generator under 0.3 mbar of oxygen and 200 W source power. Ag, Ti, Cr, Au, Sn, Au, Al, Pd thermal and e-beam deposition were tested on TCNQ to examine the adhesion to the surface, needed to withstand the removal of the non-exposed chitosan acetate film during the lift-off. The best results are illustrated in Figure S9, Supporting Information. All other metals listed above but not shown in the figure demonstrated worse adhesion and detachment of the metallic pattern during resist removal. Palladium (Pd) was a metal of choice for its good adhesion to rubrene and TCNQ.

OS Synthesis: Single crystals of rubrene and TCNQ[67] were grown by physical vapor transport in a stream of ultra-high-purity helium gas. The materials were purchased at Sigma Aldrich. Temperatures in the sublimation zone during the crystal growth were kept ≈320 and 280 °C for rubrene and TCNQ, respectively. The temperature gradient along the growth tube was ≈5 °C cm^{-1}, and the helium flow rate was 150 sccm. For the fabrication of polycrystalline rubrene thin films, Si/polyimide substrates coated with ITO, aluminum oxide (100 nm) and TPTPA (5 nm) were prepared by following the previously published procedure.[39] Rubrene (sublimed grade, Nichem, USA) was deposited by thermal evaporation (20 nm), followed by annealing on a hot plate at 140 °C for 6 min in a nitrogen atmosphere.

OS Stability: Rubrene is a relatively inert aromatic compound. It oxidizes and reduces reversibly at 0.95 and −1.37 V, respectively versus saturated calomel electrode.[41] Thus, it could not react with common aldehydes and carboxylic acids like formic acid directly without preliminary formation of radical anion or cation of rubrene while interacting with the reagents. In turn, $NiCl_2$ was often utilized as a catalyst for chloride transfer and/or a source of chloride anion. The formation of coordinative compounds with Ni^{2+} was defined by nucleophilic properties of a ligand and could be observed in the case of molecules, which exhibit high nucleophilicity like acetylacetone, dimethoxyethane, ammonia, etc. Rubrene could be hardly considered a nucleophile owing to the strong delocalization of electron density in the π-system. Such an interaction could be suggested only with rubrene anions. However, the latter can be formed only in the presence of strong reducers in the system, which was excluded in our experiments. Concerning TCNQ, there is a possibility[42] of the coordination complex formation with Ni ions. However, our experiments revealed no morphological change of the crystal surface after a radiation exposure and $NiCl_2$ solution treatment (see Figure 4). Since TCNQ used in our research is a molecular crystal, formation of the complex compound would have inevitably resulted in the materials loss. As far as the interaction of the crystal surface occurs only during the development, one would have been able to detect the morphological change with the help of AFM. Finally, the experimental conditions significantly differ from the conditions in the published evidence of the TCNQ-Ni complex compound formation.

FET Fabrication: Several individual SWCNTs and their small bundles were identified and located using an AFM relative to markers. The rest of the tubes were etched away by oxygen plasma, keeping chosen SWCNTs covered by the resist. Chitosan acetate was spin-coated and e-beam lithography was performed followed by two-step development, with the subsequent deposition of Ti (5 Å) and Pd (15 nm) contacts via e-beam evaporation. For the case of OFETs, two-step development chitosan-based lithography was similarly performed with subsequent deposition of 12 nm Pd layer and lift-off. For all cases lift-off was performed by 0.1% formic acid aqueous solution.

Brain Microtubule Patterning: 99% pure porcine brain pre-formed microtubules MT-002-A (Cytoskeleton, USA) were resuspended according to the protocol in 15 mM HEPES buffer (pH = 7.0) with 1 mM $MgCl_2$ and 30 µL of 2 mM paclitaxel solution in DMSO. Afterward, Si/SiO_2 (300 nm SiO_2 thickness) substrate with landmarks was processed in oxygen plasma and covered with the solution containing the microtubules, left for 15 min, thoroughly washed with MQ water and air dried. Microtubules were localized relative to the landmarks with the help of an AFM operating in PeakForce tapping regime with a fixed load at 1–2.5 nN. Chitosan acetate resist based e-beam lithography was performed, utilizing two-step development approach. Cr (1 nm)/Pd (24 nm) contacts were thermally evaporated, and the chip was subjected to the lift-off procedure in 0.1% formic acid solution.

Electrical Measurements: Measurements of OFETs' characteristics were performed under ambient conditions with a Keysight B1500A Semiconductor Analyzer equipped with two high rate source-measure units and a probe station. For measurements in vacuum (below 4×10^{-5} Torr), the sample holders were wire-bonded with Al wire on a home-built chipholder system connected to a BNC output. SWCNT-FETs were measured with the help of MFLI lock-in and 10^8 A/V transimpedance amplifier connected to Bruker Nanoscope V controller ADC. Four-probe microtubule devices were investigated with the help of B1500A Semiconductor Analyzer (DC measurements), MFIA Impedance analyzer (frequency range from 1 Hz to 5 MHz) and NI-5632 Vector Network Analyzer (frequency range from 300 kHz to 8.5 GHz). For all data obtained with VNA, 0 dBm input power was used.

Supporting Information

Supporting Information is available from the Wiley Online Library or from the author.

Acknowledgements

A.G. and A.B. contributed equally to this work. The authors thank Andrey Starkov for the help with illustrations and Dr. Ivan Shuklov for providing chemical reagents. A.G., K.M., V.D. thank the late Vsevolod Gantmakher for the inspiration and support provided at the beginning of this study. The development concept was designed under financial support by Russian Science Foundation under grant 19-73-10154. The experiments of the model developer investigation were supported by Russian Science Foundation under grant No. 18-72-10135. XPS was carried out with the support of the Research Facility Center at the Institute of Solid State Physics (RAS) (R.N.M. and A.M.I). This work was performed using equipment of MIPT Shared Facilities Center. F.S.F. acknowledges Russian Foundation for Basic Research grant no. 19-07-00300. V.P. acknowledges support from the National Science Foundation under the grant ECCS-1806363. B.P.R. and J.T.D. acknowledge support from the National Science Foundation Award No. ECCS-1709222. Section on the synthesis of chitosan acetate with various molecular weights was supported by Ministry of Science and Higher Education of the Russian Federation. A.I. expresses gratitude to the Russian Foundation for Basic Research (project no. 19-29-03021 mk) for supporting his work. A.K.G. acknowledge RFBR grant 19-32-90143. A.G.N. acknowledges the Russian Science Foundation (project No 17-19-01787-synthesis of carbon nanotubes and project No 21-72-20050-SWCNT transistor fabrication and characterisation).

Conflict of Interest

The authors declare no conflict of interest.

Data Availability Statement

The data that support the findings of this study are available from the corresponding author upon reasonable request.

Keywords

bio-nanostructures, delicate materials, lithography, organic semiconductors

Received: February 12, 2021
Revised: March 18, 2021
Published online:

[1] Y. Xu, F. Zhang, X. Feng, *Small* **2011**, *7*, 1338.
[2] A. Pron, P. Rannou, *Prog. Polym. Sci.* **2002**, *27*, 135.
[3] M. Y. El-Naggar, G. Wanger, K. M. Leung, T. D. Yuzvinsky, G. Southam, J. Yang, W. M. Lau, K. H. Nealson, Y. A. Gorby, *Proc. Natl. Acad. Sci. U. S. A.* **2010**, *107*, 18127.
[4] M. Amit, N. Ashkenasy, *Isr. J. Chem.* **2014**, *54*, 703.
[5] J. Harwell, J. Burch, A. Fikouras, M. C. Gather, A. Di Falco, I. D. W. Samuel, *ACS Nano* **2019**, *13*, 3823.
[6] P. Falcaro, D. Buso, A. J. Hill, C. M. Doherty, *Adv. Mater.* **2012**, *24*, 3153.
[7] S. Casalini, C. A. Bortolotti, F. Leonardi, F. Biscarini, *Chem. Soc. Rev.* **2017**, *46*, 40.
[8] D. Brunel, D. Troadec, D. Hourlier, D. Deresmes, M. Zdrojek, T. Mélin, *Microelectron. Eng.* **2011**, *88*, 1569.
[9] J. Park, J. Ho, H. Yun, M. Park, J. H. Lee, M. Seo, E. E. B. Campbell, C. Lee, S. Pyo, S. W. Lee, *Appl. Phys. A* **2013**, *111*, 1051.
[10] J. Jang, Y. Song, D. Yoo, C. K. Ober, J.-K. Lee, T. Lee, *Flexible Printed Electron.* **2016**, *1*, 023001.
[11] A. G. Ismail, *Org. Electron.* **2018**, *56*, 111.
[12] V. Linder, B. D. Gates, D. Ryan, B. A. Parviz, G. M. Whitesides, *Small* **2005**, *1*, 730.
[13] S. Kim, B. Marelli, M. A. Brenckle, A. N. Mitropoulos, E.-S. Gil, K. Tsioris, H. Tao, D. L. Kaplan, F. G. Omenetto, *Nat. Nanotechnol.* **2014**, *9*, 306.
[14] Y.-L. Sun, Q. Li, S.-M. Sun, J.-C. Huang, B.-Y. Zheng, Q.-D. Chen, Z.-Z. Shao, H.-B. Sun, *Nat. Commun.* **2015**, *6*, 8612.
[15] J. Park, S.-G. Lee, B. Marelli, M. Lee, T. Kim, H.-K. Oh, H. Jeon, F. G. Omenetto, S. Kim, *RSC Adv.* **2016**, *6*, 39330.
[16] H. Wang, Y. Zhang, H. Shao, X. Hu, *Int. J. Biol. Macromol.* **2005**, *36*, 66.
[17] S. Takei, A. Oshima, T. G. Oyama, K. Ito, K. Sugahara, M. Kashiwakura, T. Kozawa, S. Tagawa, M. Hanabata, *Jpn. J. Appl. Phys.* **2014**, *53*, 116505.
[18] B. Jiang, J. Yang, C. Li, L. Zhang, X. Zhang, P. Yang, *Adv. Mater. Interfaces* **2017**, *4*, 1601223.
[19] D. Wang, Y. Ha, J. Gu, Q. Li, L. Zhang, P. Yang, *Adv. Mater.* **2016**, *28*, 7414.
[20] S. S. Voznesenskiy, A. Nepomnyaschiy, Y. N. Kulchin, *Solid State Phenom.* **2014**, *213*, 180.
[21] M. Caillau, P. Crémillieu, E. Laurenceau, Y. Chevolot, J.-L. Leclercq, S. Alekseev, C. Chevalier, T. Delair, *J. Vac. Sci. Technol., B* **2017**, *35*, 06GE01.

[22] A. Pestov, S. Bratskaya, *Molecules* **2016**, *21*, 330.
[23] F. Yang, H. Liu, J. Qu, J. Paul Chen, *Bioresour. Technol.* **2011**, *102*, 2821.
[24] J. Matienzo, L. I. Yin, S. O. Grim, W. E. Swartz, *Inorg. Chem.* **1973**, *12*, 2762.
[25] N. S. McIntyre, M. G. Cook, *Anal. Chem.* **1975**, *47*, 2208.
[26] R. S. Vieira, M. L. M. Oliveira, E. Guibal, E. Rodríguez-Castellón, M. M. Beppu, *Colloids Surf., A* **2011**, *374*, 108.
[27] I. Lakhdhar, D. Belosinschi, P. Mangin, B. Chabot, *J. Environ. Chem. Eng.* **2016**, *4*, 3159.
[28] J. Li, Y. Du, H. Liang, *J. Appl. Polym. Sci.* **2006**, *102*, 1098.
[29] S. T. Koev, P. H. Dykstra, X. Luo, G. W. Rubloff, W. E. Bentley, G. F. Payne, R. Ghodssi, *Lab Chip* **2010**, *10*, 3026.
[30] S. Pradhan, S. S. Shukla, K. L. Dorris, *J. Hazard. Mater.* **2005**, *125*, 201.
[31] H. Duan, D. Winston, J. K. W. Yang, B. M. Cord, V. R. Manfrinato, K. K. Berggren, *J. Vac. Sci. Technol., B* **2010**, *28*, C6C58.
[32] M. J. Bowden, *J. Electrochem. Soc.* **1981**, *128*, 195C.
[33] K. L. Tai, R. G. Vadimsky, C. T. Kemmerer, J. S. Wagner, V. E. Lamberti, A. G. Timko, *J. Vac. Sci. Technol.* **1980**, *17*, 1169.
[34] T. A. Brunner, *J. Vac. Sci. Technol., B: Microelectron. Nanometer Struct.–Process., Meas., Phenom.* **1999**, *17*, 3362.
[35] A. Cattoni, D. Mailly, O. Dalstein, M. Faustini, G. Seniutinas, B. Rösner, C. David, *Microelectron. Eng.* **2018**, *193*, 18.
[36] W. M. Moreau, in *Semiconductor Lithography*, (Ed.: W.M. Moreau), Springer US, Boston, MA **1988**, pp. 459–544.
[37] M. Mende, D. Schwarz, C. Steinbach, R. Boldt, S. Schwarz, *Materials* **2018**, *11*, 373.
[38] E. Menard, V. Podzorov, S.-H. Hur, A. Gaur, M. E. Gershenson, J. A. Rogers, *Adv. Mater.* **2004**, *16*, 2097.
[39] M. A. Fusella, S. Yang, K. Abbasi, H. H. Choi, Z. Yao, V. Podzorov, A. Avishai, B. P. Rand, *Chem. Mater.* **2017**, *29*, 6666.
[40] H. H. Choi, A. F. Paterson, M. A. Fusella, J. Panidi, O. Solomeshch, N. Tessler, M. Heeney, K. Cho, T. D. Anthopoulos, B. P. Rand, V. Podzorov, *Adv. Funct. Mater.* **2019**, *30*, 1903617.
[41] D. L. Maricle, A. Maurer, *J. Am. Chem. Soc.* **1967**, *89*, 188.
[42] L. Ballester, A. Gutiérrez, M. F. Perpiñán, A. E. Sánchez, M. Fonari, M. Gdaniec, *Inorg. Chem.* **2007**, *46*, 3946.
[43] S. Iijima, T. Ichihashi, *Nature* **1993**, *363*, 603.
[44] A. Goldoni, R. Larciprete, L. Petaccia, S. Lizzit, *J. Am. Chem. Soc.* **2003**, *125*, 11329.
[45] A. Moisala, A. G. Nasibulin, D. P. Brown, H. Jiang, L. Khriachtchev, E. I. Kauppinen, *Chem. Eng. Sci.* **2006**, *61*, 4393.
[46] E. A. Laird, F. Kuemmeth, G. A. Steele, K. Grove-Rasmussen, J. Nygård, K. Flensberg, L. P. Kouwenhoven, *Rev. Mod. Phys.* **2015**, *87*, 703.
[47] S. U. Piatrusha, L. V. Ginzburg, E. S. Tikhonov, D. V. Shovkun, G. Koblmüller, A. V. Bubis, A. K. Grebenko, A. G. Nasibulin, V. S. Khrapai, *JETP Lett.* **2018**, *108*, 71.
[48] H. H. Choi, K. Cho, C. D. Frisbie, H. Sirringhaus, V. Podzorov, *Nat. Mater.* **2018**, *17*, 2.
[49] D. Havelka, M. Cifra, O. Kučera, *Appl. Phys. Lett.* **2014**, *104*, 243702.
[50] M. V. Satarić, J. A. Tuszyński, R. B. Žakula, *Phys. Rev. E* **1993**, *48*, 589.
[51] R. Mańka, B. Ogrodnik, *J. Biol. Phys.* **1991**, *18*, 185.
[52] S. Hameroff, R. Penrose, *Math. Comput. Simul.* **1996**, *40*, 453.
[53] M. Kent, W. Meyer, *J. Phys. D: Appl. Phys.* **1984**, *17*, 1687.
[54] A. Grebenko, V. Dremov, P. Barzilovich, A. Bubis, K. Sidoruk, T. Voeikova, Z. Gagkaeva, T. Chernov, E. Korostylev, B. Gorshunov, K. Motovilov, *PLoS One* **2018**, *13*, e0191289.
[55] K. A. Motovilov, M. Savinov, E. S. Zhukova, A. A. Pronin, Z. V. Gagkaeva, V. Grinenko, K. V. Sidoruk, T. A. Voeikova, P. Y. Barzilovich, A. K. Grebenko, S. V. Lisovskii, V. I. Torgashev, P. Bednyakov, J. Pokorný, M. Dressel, B. P. Gorshunov, *Sci. Rep.* **2017**, *7*, 15731.
[56] Q. Song, Z. Zhang, J. Gao, C. Ding, *J. Appl. Polym. Sci.* **2011**, *119*, 3282.
[57] N. A. Aziz, S. R. Majid, A. K. Arof, *J. Non-Cryst. Solids* **2012**, *358*, 1581.
[58] B. Ts. Shagdarova, A. V. Ilyina, S. A. Lopatin, M. I. Kartashov, L. R. Arslanova, V. G. Dzhavakhiya, V. P. Varlamov, *Appl. Biochem. Microbiol.* **2018**, *54*, 71.
[59] A. V. Il'ina, Y. V. Tkacheva, V. P. Varlamov, *Appl. Biochem. Microbiol.* **2002**, *38*, 112.
[60] H. A. A. El-Rehim, D. A. Zahran, N. M. El-Sawy, E.-S. A. Hegazy, A. M. Elbarbary, *Biosci., Biotechnol., Biochem.* **2015**, *79*, 997.
[61] R. Yoksan, M. Akashi, S. Biramontri, S. Chirachanchai, *Biomacromolecules* **2001**, *2*, 1038.
[62] A. Sionkowska, M. Wisniewski, J. Skopinska, G. F. Poggi, E. Marsano, C. A. Maxwell, T. J. Wess, *Polym. Degrad. Stab.* **2006**, *91*, 3026.
[63] A. G. Chmielewski, *Radiat. Phys. Chem.* **2010**, *79*, 272.
[64] M. A. García, N. de la Paz, C. Castro, J. L. Rodríguez, M. Rapado, R. Zuluaga, P. Gañán, A. Casariego, *J. Radiat. Res. Appl. Sci.* **2015**, *8*, 190.
[65] R. Ash, J. A. Barrie, *J. Appl. Polym. Sci.* **1986**, *31*, 1209.
[66] B. A. Miller-Chou, J. L. Koenig, *Prog. Polym. Sci.* **2003**, *28*, 1223.
[67] N. A. Peppas, D. L. Meadows, *J. Membr. Sci.* **1983**, *16*, 361.